Propagation of plane-wave vibrational excitations in disordered systems

S. N. Taraskin and S. R. Elliott
Department of Chemistry, University of Cambridge, Lensfield Road, Cambridge CB2 1EW, United Kingdom
(Received 11 August 1998; revised manuscript received 28 June 1999)

The propagational behavior of vibrational plane waves in a disordered medium has been analyzed theoretically in the time and frequency domains and in terms of the final scattered state in momentum space. Numerical results have been obtained for a normal-mode analysis of models of vitreous silica constructed by molecular dynamics, and also for a simple model of a zigzag chain of atoms with force-constant disorder.

I. INTRODUCTION

Propagation of classical plane waves in random scattering media has attracted a lot of theoretical and experimental attention in recent years.[1,2] Different types of plane waves including light, electron wave functions, and atomic vibrations are the subject of investigation in this respect. Below we consider only propagation of plane-wave atomic vibrational excitations in disordered systems. This topic has attracted a lot of attention from both theoretical[3–7] and experimental sides.[8–22] This is due to the fact that a study of plane-wave propagation helps to get information about vibrational dynamics of the system (e.g., about the normal modes and their properties) and allows us to investigate heat transfer in disordered structures (see, e.g., Refs. 23 and 24 and references therein).

A plane-wave vibrational excitation normally does not propagate freely in a disordered structure. It scatters and is attenuated with time. The main questions here are: what are the physical mechanisms of the scattering and what are the physical characteristics of such scattering (e.g., the decay time). Different decay channels have been suggested to explain the attenuation of plane-wave vibrational excitations in disordered structures: (i) disorder-induced channels;[7,23–26] (ii) anharmonic channels,[25] and (iii) channels involving two-level systems.[4,16,27,28] The anharmonic channels are strongly enhanced with increasing temperature, particularly at temperatures comparable with the glass-transition temperature, $T_g \sim 10^3$ K. In contrast, scattering by two-level systems can be important at low temperatures,[4] $T \ll T_{TLS} \sim 10-100$ K.[27,29] In the intermediate temperature range, $T_{TLS} \lesssim T \ll T_g$, which is considered below, the scattering processes involving two-level systems are suppressed and the atomic dynamics are usually harmonic,[7,30,31] meaning that disorder-induced channels play the most important role in the decay mechanism of plane-wave excitations.

In a harmonic solid, a powerful normal-mode analysis[32] can be used for the problem under consideration. The normal modes can be found either analytically or numerically. A general theory of atomic vibrations in disordered structures, which in principle should result in normal modes, has been mainly developed for particular simple model structures or toy models,[23,32–37] which can hardly describe quantitatively the situation in real structures. Therefore a numerical approach could be very useful in the calculation of normal modes, e.g., by direct diagonalization of the dynamical matrix which can be available, e.g., from molecular-dynamics simulations.

Our approach to investigating the propagation of plane-wave vibrational excitations in disordered media is based on combining analytical and numerical techniques. First, we create a realistic structural model of a disordered atomic material using molecular dynamics. We need such a structural model in order to find numerically all eigenmodes and eigenfrequencies (in the harmonic approximation), e.g., by direct diagonalization of the dynamical matrix. These characteristics fully determine the dynamical response of the system to any external excitations, including the plane-wave excitations of present interest. A straightforward analytical formalism assuming known eigenmodes and eigenfrequencies can be easily developed and applied to the analysis of plane-wave propagation in three complementary domains: time, frequency, and wave vector. In other words, we have investigated the evolution of plane-wave vibrational excitations in three ways: (i) by following numerically the time evolution of plane waves and calculating the decay time; (ii) by analyzing the spectral densities of the excitations in frequency space and thereby obtaining complementary estimates of the decay time; (iii) by analyzing in momentum (**k**) space (analytically and numerically) the final state after scattering from the initial plane-wave state.

The main difficulty in investigating the propagation of vibrational excitations in disordered systems by a normal-mode analysis is related to the restricted scope of numerical analyses of finite-size models. For example, for a cubic finite-sized model with a box length of $L \simeq 28$ Å (as used in this study), the minimum value of the wave vector $k_{min} = 2\pi/L$, allowed by the periodic boundary conditions is $k_{min} \simeq 0.22$ Å^{-1}. There is a corresponding restriction also on the minimum frequency ω_{min}, attainable in such finite-size simulations, given by $\omega_{min} = ck_{min}$, where c is an appropriate sound velocity. Moreover, due to finite model size, the low-frequency region of the vibrational density of states (VDOS) related to the acoustic plane-wave excitations is not dense, and hence the number of scattering (''decay'') channels of the plane waves with such frequencies is restricted (see also Refs. 26 and 38). In order to overcome this difficulty, we have extended the results of the numerical simulations obtained for finite-size models to frequencies and wave vectors below ω_{min} and k_{min}, respectively, by developing an analytical continuation model (see accompanying paper[39]), as well as studying low-dimensional ''toy'' disordered models.

In order to analyze the propagation of vibrational excitations in a realistic structural model simulating a real disordered system, namely vitreous silica (v-SiO_2), we have also undertaken a preliminary analysis of a simple ''toy''model, i.e., a zigzag chain with force-constant disorder, that exhibits qualitatively similar scattering behavior for vibrational excitations to that found from the simulations of the glass.

The rest of the paper is arranged in the following manner. Section II briefly describes details of the computer simulations of the structural models of v-SiO_2 used. The basis of the analytical consideration of the propagation behavior of vibrational plane waves is presented in Sec. III. An analysis in frequency space (in terms of spectral densities) is given in Sec. IV, and a complementary analysis in terms of the time evolution of vibrational excitations is given in Sec. V. An analysis in momentum **k** space of the final state of the scattered plane-wave excitations is presented in Sec. VI. A discussion of scattering mechanisms of plane-wave vibrational excitations and preliminary results of the scattering behavior of a disordered zigzag chain are presented in Sec. VII. The accompanying paper[39] uses techniques outlined in this paper to investigate the Ioffe-Regel crossover in v-SiO_2.

II. DETAILS OF SIMULATIONS

The models of v-SiO_2 have been constructed by N-P-T molecular-dynamics simulations, using the potential of van Beest, Kramer, and van Santen.[40] The van Beest potential has been modified for small interatomic distances according to Ref. 41. At large interatomic distances, we have used a cutoff for short-range interactions, multiplying the modified van Beest potential by a Fermi-like step function. The step function is characterized by the step position at $R_{\rm cut}=5.5$ Å and the step width $\delta R_{\rm cut}=0.5$ Å for all atomic species. The latter cutoff has been used to obtain a density of the glassy structure (at zero pressure), of 2.38 g/cm^3, reasonably close to the experimental value of 2.2 g/cm^3 (see the discussion of the densification problem in Ref. 41). Note that a similar cutoff ($R_{cut}=5.0$ Å and $\delta R_{cut}=0$) has been used in Ref. 42.

All glassy models have been created by quenching from the melt ($T=6000$ K) to the well-relaxed glassy state ($T\sim10^{-4}$ K) at an average quench rate of ~1 K/ps. No coordination defects have been found in the models. The fully dense dynamical matrices for the relaxed systems were diagonalized directly, resulting in eigenvectors $\{\mathbf{e}^j\}$ and eigenvalues (ω_j), thus allowing us to perform a complete harmonic vibrational analysis. Structural characteristics and vibrational properties of the models are very similar to those described in Ref. 43.

The models of v-SiO_2 were of two types: a cubic model containing $N=1650$ atoms and of box length $L\simeq28.4$ Å, and a bar configuration containing $N=1500$ atoms of size $85.6\times15.6\times15.6$ Å (a bar-shaped model of B_2O_3 has been also used in Ref. 44). For the sake of comparison, several models of α-cristobalite have also been created. The bar-shaped models were constructed to allow access to much lower values of $k(\gtrsim0.07$ Å$^{-1})$ for modes propagating along the bar than can be obtained for the cubic models ($k\gtrsim0.22$ Å^{-1}).

III. BASIC FORMALISM

The time evolution of any vibrational excitation is fully determined in the harmonic approximation by the eigenmodes and eigenfrequencies of the system. Indeed, the initial excitation can be expanded in the eigenmodes, the time dependence of which is known. The coefficients in such an expansion are defined by the shape of the initial vibrational excitation (by initial atomic displacements) and initial velocities of the atoms. Here we consider only plane-wave initial excitations, mainly because exactly such excitations are generated in a system by inelastic neutron, light, and electron scattering.[45]

In amorphous materials, because of disorder, the eigenmodes are not plane waves even in the long-wavelength limit. Therefore, an initial plane wave, when expanded over eigenmodes, contains different eigenmodes characterized by different weights in this expansion. The eigenmodes participating in the expansion are characterized by different eigenfrequencies and therefore evolve differently with time, so that the propagating excitation becomes different in shape compared with the initial one. On the other hand, we can always expand any vibrational state in plane waves which form another complete (but not fully orthogonal, as discussed below) basis set, i.e., make a Fourier analysis. If we do this with the evolving excitation (initially a single plane wave) after a certain time, then this expansion contains not only the initial plane-wave component but also other plane waves characterized by different wave vectors. This means that the initial plane wave is scattered by the structure into a different final state. Our aim here is to study both the process itself of decay of plane waves, and also the final state after decay, for different wave vectors and polarizations of an initial plane wave.

Let us consider an excitation introduced in the system, $\mathbf{u}(t)=\mathbf{u}_{\mathbf{k}}(t)$, which at the initial moment of time, $t=0$, is an ideal plane wave, $\mathbf{w}_{\mathbf{k},\hat{\mathbf{n}}}$, characterized by the wave vector **k**, unit polarization vector $\hat{\mathbf{n}}$ and initial phase ϕ_0:

$$\mathbf{u}_{\mathbf{k}}(t=0)=\mathbf{w}_{\mathbf{k}}\equiv A\hat{\mathbf{n}}\cos[\mathbf{k}\cdot\mathbf{r}+\phi_0], \tag{3.1}$$

where **u** is a vibrational state vector in a $3N$-dimensional linear vector space spanned by the orthonormal basis $\{\mathbf{s}_i\}$ ($i=1,\ldots,3N$), with the basis vectors being, e.g., the unit displacement vectors of a certain atom along one of the Cartesian axes (the site basis). In that case, the components of vector **u** are the displacement vectors, $\mathbf{u}_i$ ($i=1,\ldots,N$), of atoms i from their equilibrium positions, $\mathbf{r}_i$. The normalization constant A is defined below and the wave-vector index **k** includes also the polarization index $\hat{\mathbf{n}}$. In our analytical treatment, we assume that eigenmodes and eigenfrequencies are known, e.g., from numerical simulations. The initial displacement vector, Eq. (3.1), each atomic component of which is multiplied by the mass factor $m_i=M_iN/\Sigma_iM_i$ (M_i stands for the mass of atom i), can be expanded in eigenmodes as

$$\mathbf{u}_{\mathbf{k}}(0)=\sum_{j=1}^{3N}\alpha_{\mathbf{k}}^{j}\mathbf{e}^{\mathbf{j}}/\sqrt{m}, \tag{3.2}$$

where the symbolic script $\mathbf{e}^{\mathbf{j}}/\sqrt{m}$ means that each ith component of vector $\mathbf{e}^{\mathbf{j}}$ is divided by the factor $\sqrt{m_i}$. The coefficients $\overline{\alpha^j_{\mathbf{k}}}$ in expansion (3.2), the squares of which are the spectral-density coefficients of the system (see, e.g., Refs. 24 and 46), are defined by the following equation:

$$\overline{\alpha^j_{\mathbf{k}}} = \langle \mathbf{e}^j \cdot \sqrt{m}\mathbf{u}_{\mathbf{k}}(0)\rangle \equiv \sum_{i=1}^{N} \sqrt{m_i}\mathbf{e}^j_i \cdot \mathbf{w}_{\mathbf{k},i}. \tag{3.3}$$

The expansion coefficients, Eq. (3.3), fully determine the dynamical response of the system to plane-wave excitation. Indeed, at any moment of time t, the displacement vector of the propagating excitation can be represented via eigenmodes developing in time as

$$\mathbf{u}_{\mathbf{k}}(t) = \sum_{1}^{3N} \overline{\alpha^j_{\mathbf{k}}} \frac{\mathbf{e}^j}{\sqrt{m}} \cos \omega_j t. \tag{3.4}$$

For the sake of simplicity and without loss of generality (as shown below), we consider the initial excitation to be a standing wave, i.e., $\dot{\mathbf{u}}_{\mathbf{k}}(0) = 0$, leading to the absence of terms proportional to $\sin \omega_j t$ in expression (3.4). It is convenient for the initial vector $\sqrt{m}\mathbf{u}_{\mathbf{k}}(0)$ to be normalized to unity, so that

$$\sum_{1}^{3N} |\overline{\alpha^j_{\mathbf{k}}}|^2 = 1, \tag{3.5}$$

and the normalization constant in Eq. (3.1) is $A^2 = [\Sigma_i m_i |\mathbf{u}_{\mathbf{k}}(0)|^2]^{-1}$.

Equation (3.4) gives us a formal answer for the problem under investigation. Now we want to be more specific and characterize such an evolving state $\mathbf{u}_{\mathbf{k}}(t)$ in some qualitative way. The simplest thing to do is to make a Fourier analysis of this state, i.e., expand it in plane waves:

$$\mathbf{u}_{\mathbf{k}}(t) = \sum_{\mathbf{k}'} \mathbf{u}_{\mathbf{k}\mathbf{k}'}(t), \tag{3.6}$$

where the sum is taken over all wave vectors $\mathbf{k}'$ (allowed by the periodic simulation box in the case of a finite model) and all polarizations (two transverse and one longitudinal for each wave vector) with $\mathbf{k}$ being the wave vector of the initial plane wave. Such an expansion gives us an opportunity to calculate the weights of different plane-wave components in the propagating excitation, which appear in it due to scattering.

The waves $\mathbf{u}_{\mathbf{k}\mathbf{k}'}(t)$ in Eq. (3.6) are defined as

$$\mathbf{u}_{\mathbf{k}\mathbf{k}'}(t) = a_{\mathbf{k}\mathbf{k}'}(t) A \hat{\mathbf{n}}' \cos[\mathbf{k}' \cdot \mathbf{r} + \phi_{\mathbf{k}\mathbf{k}'}(t)]. \tag{3.7}$$

The same normalization as in Eq. (3.1) is used here. In order to find the time dependence of the amplitude $a_{\mathbf{k}\mathbf{k}'}(t)$ and phase $\phi_{\mathbf{k}\mathbf{k}'}(t)$, it is convenient to rewrite Eq. (3.7) in the following form:

$$\mathbf{u}_{\mathbf{k}\mathbf{k}'}(t) = a_{\mathbf{k}\mathbf{k}',\mathrm{c}}(t)\mathbf{w}_{\mathbf{k}',\mathrm{c}} + a_{\mathbf{k}\mathbf{k}',\mathrm{s}}(t)\mathbf{w}_{\mathbf{k}',\mathrm{s}}, \tag{3.8}$$

where

$$\mathbf{w}_{\mathbf{k}',\mathrm{c}} = A\hat{\mathbf{n}}' \cos \mathbf{k}' \cdot \mathbf{r} \quad \text{and} \quad \mathbf{w}_{\mathbf{k}',\mathrm{s}} = A\hat{\mathbf{n}}' \sin \mathbf{k}' \cdot \mathbf{r}, \tag{3.9}$$

so that

$$a_{\mathbf{k}\mathbf{k}'}(t) = [a^2_{\mathbf{k}\mathbf{k}',\mathrm{c}}(t) + a^2_{\mathbf{k}\mathbf{k}',\mathrm{s}}(t)]^{1/2}, \tag{3.10}$$

$$\phi_{\mathbf{k}\mathbf{k}'}(t) = \arctan[a_{\mathbf{k}\mathbf{k}',\mathrm{s}}(t)/a_{\mathbf{k}\mathbf{k}',\mathrm{c}}(t)]. \tag{3.11}$$

Strictly speaking, the set of plane waves $\{\mathbf{w}_{\mathbf{k}}\}$ used in expansion (3.6) is not orthogonal because these plane waves are defined in terms of discrete disordered atomic coordinates. This drawback can be easily overcome by considering the orthonormal basis $\{\tilde{\mathbf{w}}_{\mathbf{k}}\}$ obtained from the original plane-wave basis $\{\mathbf{w}_{\mathbf{k}}\}$, e.g., by standard Gramm-Schmidt (GS) orthogonalization. Indeed, the overlap integrals $\langle \mathbf{w}_{\mathbf{k}}\mathbf{w}_{\mathbf{k}'}\rangle$ between plane waves are macroscopically small,

$$\frac{\langle \mathbf{w}_{\mathbf{k}}\mathbf{w}_{\mathbf{k}'}\rangle}{\langle \mathbf{w}_{\mathbf{k}}\mathbf{w}_{\mathbf{k}}\rangle} = \frac{1}{\mathbf{w}^2_{\mathbf{k}}} \sum_i \mathbf{w}_{\mathbf{k},i}\mathbf{w}_{\mathbf{k}',i} \propto \frac{1}{\sqrt{N}}, \tag{3.12}$$

because of summing random numbers. Bearing in mind Eq. (3.12), we can easily find an approximate relation for the wave $\tilde{\mathbf{w}}_{\mathbf{k}} = \{\tilde{\mathbf{w}}_{\mathbf{k},i}\}$ from the orthogonal set,

$$\tilde{\mathbf{w}}_{\mathbf{k},i} \simeq \mathbf{w}_{\mathbf{k},i}\left(1 - \sum_{\mathbf{k}'} \frac{\langle \mathbf{w}_{\mathbf{k}'}\mathbf{w}_{\mathbf{k}}\rangle}{\langle \mathbf{w}_{\mathbf{k}'}\mathbf{w}_{\mathbf{k}'}\rangle} \frac{\mathbf{w}_{\mathbf{k}',i}}{\mathbf{w}_{\mathbf{k},i}}\right). \tag{3.13}$$

The shape of wave $\tilde{\mathbf{w}}_{\mathbf{k}}$ is close to the shape of $\mathbf{w}_{\mathbf{k}}$ if the sum in Eq. (3.13) is much less than unity. This is the case if the number of waves $N_{\mathrm{orth}}(k)$ involved in the orthogonalization, i.e., the number of terms in the sum in Eq. (3.13), is small enough. Indeed, if we start the GS orthogonalization with plane waves characterized by the smallest wave-vector magnitude and then carry on by including waves according to their increasing wave-vector magnitude $|\mathbf{k}|$, then the sum in Eq. (3.13) includes all waves with $|\mathbf{k}'| \lesssim k$, i.e., $N_{\mathrm{orth}}(k) \propto k^3$. Taking into account that $\mathbf{w}_{\mathbf{k}',i}/\mathbf{w}_{\mathbf{k},i}$ are random values being order of unity and using Eq. (3.12) we can easily obtain an estimate for the sum in Eq. (3.13), $\Sigma_{\mathbf{k}'} \propto [N_{\mathrm{orth}}(k)/N_{\mathrm{tot}}(k_{\max})]^{1/2} \propto (k/k_{\max})^{3/2}$, with $N_{\mathrm{tot}} = 3N$ being the total number of waves in the set and $k_{\max} \approx \pi/a$ the typical maximum wave-vector magnitude (a is the average interatomic distance). Therefore the shape of the orthogonal waves $\tilde{\mathbf{w}}_{\mathbf{k}}$ is close to the shape of the plane waves $\mathbf{w}_{\mathbf{k}}$ if $k \lesssim k_*$, with the value of k_* chosen such that inequality $(k_*/k_{\max})^{3/2} \ll 1$ is satisfied. For the particular case of vitreous silica, a reasonable estimate of the upper limit of our consideration in k space is $k_* \simeq 1$ Å^{-1} as compared to $k_{\max} \simeq 1.7$ Å^{-1}. This means that two sets, non-orthogonal plane waves and corresponding orthonormal GS waves, are equivalent in the range $k \lesssim k_*$ in the sense that all physical characteristics (e.g., spectral densities, ρ functions, etc.) are practically identical, as we have checked numerically. All the results presented below, unless specifically mentioned, were obtained for the plane-wave basis.

Now we would like to find the time-dependent coefficients $a_{\mathbf{k}\mathbf{k}',\mathrm{c(s)}}(t)$ before the cos- (sin-) like components in Eq. (3.6). This can be easily done by multiplying both sides of this equation by $\mathbf{w}_{\mathbf{k}',\mathrm{c(s)}}$ and using Eq. (3.4), so that

$$a_{\mathbf{k}\mathbf{k}',\mathrm{c(s)}}(t) = \sum_j \overline{\alpha^j_{\mathbf{k}}}\alpha^j_{\mathbf{k}',\mathrm{c(s)}} \cos \omega_j t / \langle \mathbf{w}^2_{\mathbf{k}',\mathrm{c(s)}}\rangle, \tag{3.14}$$

where

$$\langle \mathbf{w}^2_{\mathbf{k}',c(s)}\rangle \equiv \sum_{i=1}^{N} |(\mathbf{w}_{\mathbf{k}',c(s)})_i|^2. \tag{3.15}$$

The coefficients $\underline{\alpha}^j_{\mathbf{k}',c(s)}$ for plane waves of cos- and sin-like type entering the expression (3.14) are similar to $\overline{\alpha}^j_{\mathbf{k}}$ except that the eigenvectors are weighted differently with the atomic masses:

$$\underline{\alpha}^j_{\mathbf{k}',c(s)} = \left\langle \mathbf{e}^j \cdot \frac{1}{\sqrt{m}} \mathbf{w}_{\mathbf{k}',c(s)} \right\rangle \equiv \sum_{i=1}^{N} \frac{1}{\sqrt{m_i}} \mathbf{e}^j_i \cdot (\mathbf{w}_{\mathbf{k}',c(s)})_i . \tag{3.16}$$

They are also differently normalized:

$$\sum_{j=1}^{3N} |\underline{\alpha}^j_{\mathbf{k},c(s)}|^2 = \frac{\sum_i (m_i)^{-1} |\mathbf{w}_{\mathbf{k},c(s)}|^2}{\sum_i m_i |\mathbf{w}_{\mathbf{k},c(s)}|^2}, \tag{3.17}$$

as compared to the expansion coefficients $\underline{\alpha}^j_{\mathbf{k},c(s)}$ [cf. Eq. (3.5)]. In a single-component system, $\Sigma_{j=1}^{3N} |\underline{\alpha}^j_{\mathbf{k},c(s)}|^2 = \Sigma_1^{3N} |\overline{\alpha}^j_{\mathbf{k}}|^2 = 1$, but in a multicomponent system the normalization constant (3.17) is not necessarily unity, and, e.g., in the case of vitreous silica it has the value $\simeq 0.7$.

Equations (3.10)–(3.17) fully determine the time evolution of different $\mathbf{k}'$ plane-wave components in the propagating vibrational excitation via the coefficients $\overline{\alpha}^j_{\mathbf{k}}$ and $\underline{\alpha}^j_{\mathbf{k}',c(s)}$ and the vibrational spectrum itself. These equations will be used for the numerical analysis undertaken below. The next step which can be done analytically is related to the time averaging in Eqs. (3.10)–(3.17). For example, averaging the square of Eq. (3.10) as $t \to \infty$ gives us $\overline{a^2_{\mathbf{k}\mathbf{k}'}(t)}$, the weight of the plane-wave component characterized by the wave vector $\mathbf{k}'$ and polarization $\hat{\mathbf{n}}'$ in the final state if the initial state is a plane wave characterized by $\mathbf{k}$ and $\hat{\mathbf{n}}$:

$$\overline{a^2_{\mathbf{k}\mathbf{k}'}(t)} \simeq \frac{1}{2} \left\{ \frac{\sum_j |\overline{\alpha}^j_{\mathbf{k}}|^2 |\underline{\alpha}^j_{\mathbf{k}',s}|^2}{(\langle \mathbf{w}^2_{\mathbf{k}',s}\rangle)^2} + \frac{\sum_j |\overline{\alpha}^j_{\mathbf{k}}|^2 |\underline{\alpha}^j_{\mathbf{k}',c}|^2}{(\langle \mathbf{w}^2_{\mathbf{k}',c}\rangle)^2} \right\}, \tag{3.18}$$

where, as in Eq. (3.1) and subsequently, the wave-vector index $\mathbf{k}'$ also includes the polarization index $\hat{\mathbf{n}}'$. This weight is proportional to the functions $|\overline{\alpha}^j_{\mathbf{k}}|^2$ and $|\underline{\alpha}^j_{\mathbf{k}}|^2$ which play an important role in the following analysis and are called the spectral-density coefficients (see also Refs. 24 and 46).

Another useful characteristic often used to characterize the decay of an initial excitation is the time correlation function,[47]

$$\frac{\langle \mathbf{u}(t)\cdot\mathbf{u}(0)\rangle}{\langle \mathbf{u}(0)\cdot\mathbf{u}(0)\rangle} \equiv \frac{\sum_i \mathbf{u}_i(t)\mathbf{u}_i(0)}{\sum_i \mathbf{w}_{\mathbf{k},i}\mathbf{w}_{\mathbf{k},i}} = \frac{\sum_j \overline{\alpha}^j_{\mathbf{k}} \underline{\alpha}^j_{\mathbf{k}} \cos \omega_j t}{\langle \mathbf{w}^2_{\mathbf{k}}\rangle}. \tag{3.19}$$

This correlation function describes the dephasing of the initial wave and can be used to estimate the typical time of such dephasing. The coefficient $\underline{\alpha}^j_{\mathbf{k}}$ in Eq. (3.19) is defined by Eq. (3.16) with $\mathbf{w}_{\mathbf{k},c(s)}$ replaced by $\mathbf{w}_{\mathbf{k}}$, and is related to the coefficient $\overline{\alpha}^j_{\mathbf{k}}$ according to the following equation:

$$\underline{\alpha}^j_{\mathbf{k}} = \sum_{j'} \overline{\alpha}^{j'}_{\mathbf{k}} \langle \mathbf{e}^j m^{-1} \mathbf{e}^{j'} \rangle. \tag{3.20}$$

In the case of a one-component system, the coefficients $\underline{\alpha}^j_{\mathbf{k}}$ and $\overline{\alpha}^j_{\mathbf{k}}$ are obviously identical. Their product, $\overline{\alpha}^j_{\mathbf{k}} \underline{\alpha}^j_{\mathbf{k}}$, is also called the spectral-density coefficient.

The general characteristics of plane-wave propagation defined in this section can be used for quantitative (numerical) analysis. How to do this is demonstrated in the rest of the paper.

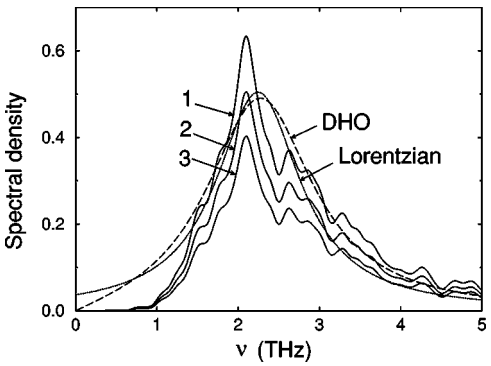

FIG. 1. Different spectral densities $\overline{S_{\mathbf{k}}}(\nu)$ (curve 1), $S_{\mathbf{k}}(\nu)$ (curve 2), and $\underline{S}_{\mathbf{k}}(\nu)$ (curve 3) for a longitudinal initial plane wave characterized by the wave-vector magnitude $k = 0.3$ Å^{-1}. The dotted line represents the fit of $\overline{S_{\mathbf{k}}}(\nu)$ by a Lorentzian [Eq. (4.8)] while the dashed line refers to a fit by the DHO model (Refs. 7 and 13).

IV. SPECTRAL DENSITIES

The coefficients $\overline{\alpha}^j_{\mathbf{k}}$, $\underline{\alpha}^j_{\mathbf{k}}$ in the expansion of different $\mathbf{k}$-plane waves over the eigenmodes, i.e., projections of plane waves onto eigenvectors, and related spectral-density coefficients $|\underline{\alpha}^j_{\mathbf{k}}|^2$, $|\overline{\alpha}^j_{\mathbf{k}}|^2$, and $\overline{\alpha}^j_{\mathbf{k}} \underline{\alpha}^j_{\mathbf{k}}$ fully determine the dynamical response of the system to the initial plane-wave excitation. These three spectral-density coefficients differ from each other due to different contributions in the coefficients $\overline{\alpha}^j_{\mathbf{k}}$ and $\underline{\alpha}^j_{\mathbf{k}}$ of the mass factor [which is not unity in multicomponent systems—see Eqs. (3.3) and (3.16)]. In the case of vitreous silica, the masses of the atomic species are quite comparable and the mass factor is of the order of unity, so that the different types of the spectral-density coefficients differ only slightly from each other. In Fig. 1, we show $|\overline{\alpha}^j_{\mathbf{k}}|^2$, $|\underline{\alpha}^j_{\mathbf{k}}|^2$, and $\overline{\alpha}^j_{\mathbf{k}} \underline{\alpha}^j_{\mathbf{k}}$ for a longitudinal initial plane wave characterized by $k = 0.3$ Å^{-1} (here, and in what follows, all the simulated data, if not mentioned explicitly, are presented for the bar-shaped structural model of v-SiO_2). It appears (see below) that the frequency dependences of the spectral-density coefficients are very similar to each other and the following approximate relationships can be used:

$$|\underline{\alpha}^j_{\mathbf{k}}|^2 \simeq A_1 |\overline{\alpha}^j_{\mathbf{k}}|^2 \quad \text{and} \quad \overline{\alpha}^j_{\mathbf{k}} \underline{\alpha}^j_{\mathbf{k}} \simeq A_2 |\overline{\alpha}^j_{\mathbf{k}}|^2, \tag{4.1}$$

with the normalization constants for the corresponding spectral-density coefficients being

$$A_1=\sum_j |\underline{\alpha}_{\mathbf{k}}^j|^2, \tag{4.2}$$

$$A_2=\sum_j \overline{\alpha}_{\mathbf{k}}^j \underline{\alpha}_{\mathbf{k}}^j, \tag{4.3}$$

which, in the case of vitreous silica, give $A_1 \simeq 0.7$ and $A_2 \simeq 0.8$. Relations (4.1) are valid, as we checked numerically, in the low- and intermediate-frequency range ($\nu \lesssim 30$ THz) but break down in the region of the high-frequency band of v-SiO_2 at $\nu \lesssim 30$ THz. However, at the not very large values of wave vector $k \lesssim k_* \simeq 1$ Å^{-1}, which we consider, the spectral-density coefficients are not mainly concentrated in the high-frequency region (see below) and the relationships (4.1) are approximately correct.

The spectral-density coefficients $|\overline{\alpha}_{\mathbf{k}}^j|^2$ contribute to the function $\overline{a_{\mathbf{kk}'}^2(t)}$ [see Eq. (3.18)] and, together with $|\underline{\alpha}_{\mathbf{k}}^j|^2$, define the properties of the final state. The distribution function $\overline{\alpha}_{\mathbf{k}}^j \underline{\alpha}_{\mathbf{k}}^j$ defines the decay of the time correlation function given by Eq. (3.19). The spectral-density coefficients $|\underline{\alpha}_{\mathbf{k}}^j|^2$ are also important from an experimental point of view, because the dynamical structure factor measured in inelastic neutron- and x-ray-scattering (IXS) experiments is proportional to them.[45] In what follows, we mainly refer to the spectral-density coefficients $|\overline{\alpha}_{\mathbf{k}}^j|^2$, taking into consideration that relations (4.1) are fulfilled.

The spectral-density coefficients are defined for discrete frequencies only. The standard transformation to the spectral-density functions $\overline{S}_{\mathbf{k}}(\omega)$, $S_{\mathbf{k}}(\omega)$, and $\underline{S}_{\mathbf{k}}(\omega)$ defined in the whole frequency range can be made as follows:[46]

$$\overline{S}_{\mathbf{k}}(\omega)=g(\omega)|\overline{\alpha}_{\mathbf{k}}(\omega)|^2, \quad S_{\mathbf{k}}(\omega)=g(\omega)\overline{\alpha}_{\mathbf{k}}^j(\omega)\underline{\alpha}_{\mathbf{k}}^j(\omega)$$
$$\text{and} \quad \underline{S}_{\mathbf{k}}(\omega)=g(\omega)|\underline{\alpha}_{\mathbf{k}}(\omega)|^2, \tag{4.4}$$

where, e.g., $|\overline{\alpha}_{\mathbf{k}}(\omega)|^2$ is defined as

$$|\overline{\alpha}_{\mathbf{k}}(\omega)|^2=\frac{\sum_{j=1}^{3N} |\overline{\alpha}_{\mathbf{k}}^j|^2 \delta(\omega-\omega^j)}{3Ng(\omega)}, \tag{4.5}$$

and $g(\omega)=\Sigma_{j=1}^{3N}\delta(\omega-\omega^j)/3N$ is the VDOS. The spectral densities are continuous functions if Gaussians (or Lorentzians) are used instead of the δ function representation in Eq. (4.5). Exactly these functions are presented in Fig. 1 and everywhere below unless specified. As seen from Fig. 1, different spectral densities have similar frequency dependences thus confirming relations (4.1).

The shape of the spectral density depends on the characteristics of the plane wave (wave vector and polarization) and on the atomic structure itself. In disordered structures and for small values of the wave-vector magnitude ($ka \ll 1$), the spectral density both for longitudinal and transverse polarizations has the shape of a single pronounced peak [see Figs. 2(a) and 2(d)]. With an increase of the magnitude k of the wave vector, the peak-shaped spectral density shifts to higher frequencies and its width increases [see Figs. 2(b) and 2(e)]. At large enough $k \gtrsim k_* \simeq 1$ Å^{-1}, the spectral density no longer consists of a single peak but rather resembles the vibrational density of states (VDOS) [see Figs. 2(c) and 2(f)], clearly showing the two frequency bands found in v-SiO_2.[43] We should notice that the range $k \gtrsim k_*$ is outside the limits of our consideration and the results there could serve as rough esimates only. Indeed, for the wave vectors around $k \simeq k_*$, the GS orthonormal states still resemble the original nonorthogonal plane waves [see Fig. 3(b)] and the spectral densities calculated for both of them are close to each other [cf. the solid and dashed curves in

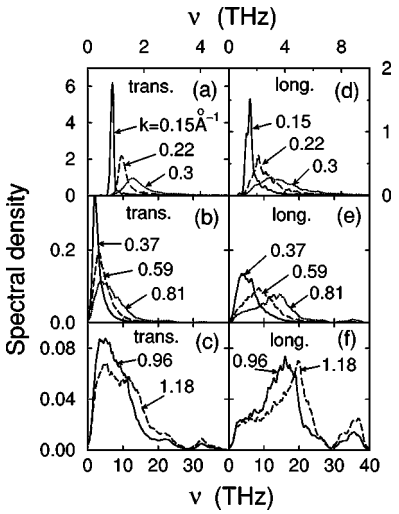

FIG. 2. The spectral densities $\overline{S}_{\mathbf{k}}(\nu)$ for transverse [(a), (b), and (c)] and longitudinal [(d), (e), and (f)] initial polarizations at different magnitudes k of the initial wave vector as shown in the figure.

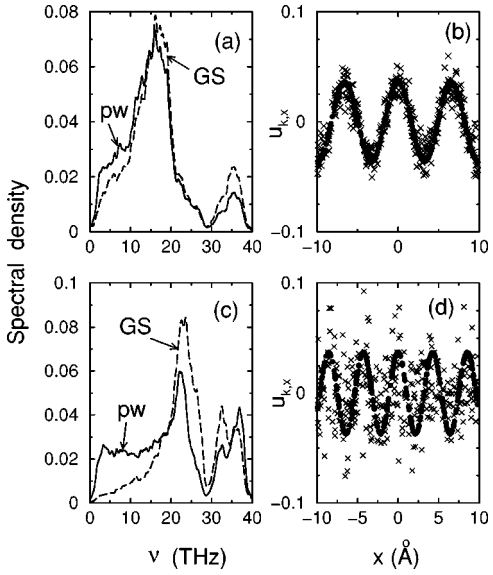

FIG. 3. The spectral densities $\overline{S}_{\mathbf{k}}(\nu)$ for plane wave (solid lines) and for the corresponding Gramm-Schmidt orthonormal state (dashed lines) of longitudinal initial polarization at different magnitudes, $k \gtrsim k_*$, of the initial wave vector: (a) $k=0.96$ Å^{-1} and (c) $k=1.47$ Å^{-1}. A part of the displacement pattern for a longitudinal plane wave (solid circles) and the corresponding Gramm-Schmidt orthonormal state (crosses) are shown for (b) $k=0.96$ Å^{-1} and (d) $k=1.47$ Å^{-1}.

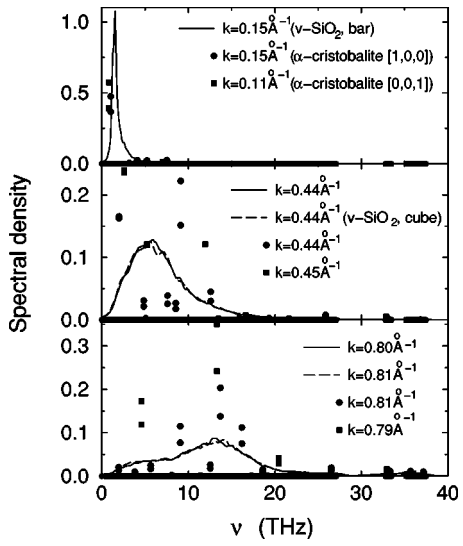

FIG. 4. The spectral densities $\overline{S_{\mathbf{k}}}(\nu)$ for longitudinal vibrations for different structural models of v-SiO_2 and similar spectral-density coefficients $|\overline{\alpha_{\mathbf{k}}^l}|^2$ for α-cristobalite at various values of wave vector k. The meaning of the symbols and curves in the lower two panels is the same as in the top panel.

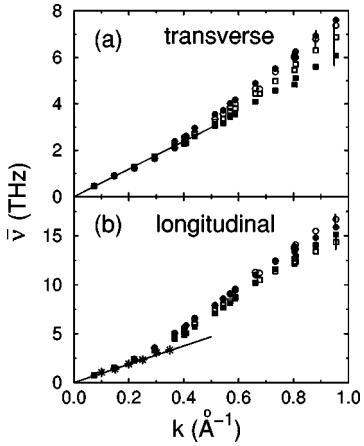

FIG. 5. The dispersion laws for transverse (a) and longitudinal (b) polarizations of an initial plane-wave excitation. The solid circles and squares were obtained from the fit of the spectral densities by Lorentzians and the DHO model, respectively. The open squares were obtained by the temporal decay method as described in Sec. V. The open circles were calculated according to Eq. (5.3). The stars in (b) correspond to IXS data (Ref. 13). The solid lines represent the long-wavelength limit characterized by the experimentally found sound velocities.

Fig. 3(a)]. The situation becomes much worse with increasing k [see Fig. 3(c)], because the GS orthonormal states for such wave vectors are not so similar to the original plane waves [see Fig. 3(d)].

In an attempt to understand the origin of changes in the shape of the spectral densities and the origin of a particular shape itself, we calculated these quantities for a crystalline counterpart of vitreous silica, namely α-cristobalite, and compared them to those for v-SiO_2 (see Fig. 4). At very small wave vectors, $k \ll \pi/a$ (a is a typical size of the unit cell, $a \simeq 5-7$ Å), the spectral density is a single δ function [see Fig. 4(a)], meaning that long-wavelength plane waves give the major contribution to acoustic phonons, which are very similar to plane waves. With increasing k, the contributions of plane waves to acoustic phonons become shared with increasing contributions from optic phonons, and at $k \gtrsim \pi/a$ (e.g., $k \gtrsim 0.3$ Å^{-1} for longitudinal branches) they are of the same order [see Figs. 4(b) and 4(c)]. Thus the spectral density for an amorphous solid (v-SiO_2) can be imagined as being a directional average over the δ functions for the corresponding crystal (α-cristobalite), each δ function being broadened by structural disorder. Dove *et al.*[48] have also discussed the relationship between the low-frequency dynamics of α-cristobalite and those of amorphous silicates.

In the low-frequency regime, where the spectral densities have the shapes of pronounced peaks, the positions of these peaks, $\nu_{t,l}$, are related to the wave-vector magnitude according to the linear relation (see Fig. 5)

$$\nu_{t,l} \simeq c_{t,l} k/2\pi, \tag{4.6}$$

as for acoustic waves in crystals. As seen from Fig. 5, the calculated dots in the low-frequency range lie on the straight lines plotted with use of experimentally found sound velocities [$c_t \simeq 37.5$ Å/ps and $c_l \simeq 59$ Å/ps (Refs. 13 and 49)]. A microscopic structure on the interatomic scale a (ordered or disordered) is not important in this frequency regime where the wavelength $\lambda \gg a$ and plane waves propagate in an effectively elastic continuum. Therefore it is not surprising to find a linear dispersion (4.6) for a disordered material if $\lambda \gg a$.

If the spectral densities are peak shaped, two of their characteristics, the peak position and width, are normally used in order to describe the propagation of plane-wave excitations.[7,12,13,24] The peak position is associated with the average frequency of the propagating excitation, while the peak width is associated with the decay time of the excitation. Indeed, if we look at the **k**-plane-wave component in the propagating excitation, $\mathbf{u}(t)$, its evolution with time is described by relation (3.7) at $\mathbf{k}' = \mathbf{k}$. The weight (amplitude) of this component, $a_{\mathbf{kk}}(t)$, decays with time according to Eqs. (3.10) and (3.14). A rough estimate of the time dependence of $a_{\mathbf{kk}}(t)$ can be obtained if we assume that $a_{\mathbf{kk}}(t) \propto a_{\mathbf{kk},c}(t)$, i.e., $a_{\mathbf{kk}}(t)$ is approximately the back cosine Fourier transformation of the spectral-density coefficients $\overline{\alpha_{\mathbf{k}}^l \alpha_{\mathbf{k}}^j}$ [see Eq. (3.14)]. If the spectral density has the shape of a well-defined peak which can be fitted, say, by a Lorentzian (see the dotted line in Fig. 1), i.e.,

$$f_L = \frac{1}{\pi} \frac{(\Gamma_\omega/2)}{(\omega - \overline{\omega_k})^2 + (\Gamma_\omega/2)^2}, \tag{4.7}$$

where the Lorentzian position $\overline{\omega_k}$ and full width at half maximum (FWHM) Γ_ω are the fitting parameters, then the back cosine Fourier transform of the function (4.7) is

$$a_{\mathbf{kk}}(t) \simeq A_2 \cos \overline{\omega_k} t \exp\{-\Gamma_\omega t/2\}, \tag{4.8}$$

where we have actually used Eq. (4.7) to fit the spectral density $\overline{S_{\mathbf{k}}}$ normalized to unity and then applied Eq. (4.1) with spectral-density coefficients replaced by the spectral densities themselves. As clearly seen from Eq. (4.8), the decay of the **k**-plane-wave component can be characterized by the average radial frequency $\overline{\omega_k}$ and the inverse decay time

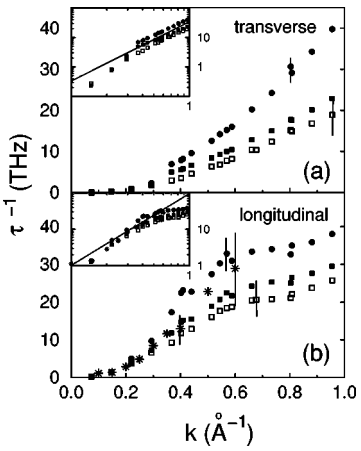

FIG. 6. Inverse decay time τ^{-1} versus the initial wave-vector magnitude k for transverse (a) and longitudinal (b) initial polarizations. The same symbols are used as in Fig. 5. In the insets, the data are plotted on a double logarithmic scale in order to compare them with the quadratic dependence shown by solid lines. The error bars were obtained from the averaging of the results over initial phase ϕ_0 and direction of the polarization $\hat{\mathbf{n}}$ (for transverse polarization) of the initial wave [see Eq. (3.1)].

$$\tau_k^{-1} \simeq \Gamma_\omega(k)/2 = \pi \Gamma_\nu(k), \tag{4.9}$$

with $\Gamma_\nu(\mathrm{THz}) = \Gamma_\omega / 2\pi$.

In Refs. 7 and 13, the damped harmonic oscillator (DHO) model has been used to fit spectral densities (see the dashed line in Fig. 1), which gives similar values for the average frequency and width, if $(\Gamma_\omega)^2 \ll \overline{\omega_k^2}$. This inequality holds true in the region $k \lesssim k_* \simeq 1$ Å^{-1} where the spectral densities have a well-defined peak shape and fitting of the spectral densities by Lorentzian and/or DHO curves makes sense.

We have used fits both by the Lorentzian and DHO models to obtain the average frequency and decay time of the propagating plane-wave excitation as a function of the initial wave vector. The results are presented in Figs. 5 and 6. The dependence of $\overline{\nu_k} = \overline{\omega_k}/2\pi$ vs k shown in Fig. 5 can be associated with some sort of ''dispersion law.'' Of course, the propagating excitation, which was a plane wave at the initial moment of time, cannot be characterized by only one wave vector (and single frequency) and instead consists of a packet of plane waves [see Eq. (3.6)] with different wave vectors (a packet of eigenmodes characterized by different frequencies). We chose from the $\mathbf{k}'$ packet only one component characterized by the same wave vector as that of the initial plane wave and followed its time evolution. In that case, the dependencies $\overline{\nu_k}$ presented in Fig. 5 can be regarded as the dispersion laws for a single plane-wave component. The experimental data for longitudinal external plane-wave excitations from IXS experiments,[13] obtained by fitting the experimental curves with the DHO model, are shown by the stars in Fig. 5(b) and they agree well with our results (see also Ref. 7).

Note that the dispersion laws for both branches are practically linear in the low-frequency (long-wavelength) regime for $\nu \lesssim 3$ THz. Above this frequency, a sort of ''fast-sound'' behavior is observed. The increase in the slope of $\overline{\nu_k}$ is related to changes in the shape of the spectral densities. A shoulder on the high-frequency side of the spectral-density peak for the longitudinal branch starts to appear at $k \gtrsim 0.3$ Å^{-1} [$\nu \gtrsim 0.3$ THz—see Figs. 2(d) and 2(e)]. A similar transformation happens with the peak for the transverse branch at $k \gtrsim 0.5$ Å^{-1}.

The width of the spectral density, as mentioned above [see Eq. (4.9)], defines the decay time of the plane-wave excitation. In Fig. 6, we have plotted the inverse decay time, which is proportional to the peak width, against wave-vector magnitude for both polarizations of the initial plane-wave excitation. As follows from the insets in Fig. 6, the inverse decay time increases with increasing k approximately proportional to k^2 for $0.2 \lesssim k \lesssim 0.5$ Å^{-1} for the longitudinal branch and for $0.3 \lesssim k \lesssim 1$ Å^{-1} in the case of the transverse branch. The first two points for the transverse branch obtained at $k \simeq 0.07$ and $\simeq 0.15$ Å^{-1} and the first point for the longitudinal branch, for which the corresponding frequencies are below $\lesssim 1$ THz, serve only as estimates of the decay time due to finite-size limitations. Such a quadratic dependence on wave-vector magnitude has been found not only in the IXS experiments in the range $k \sim 0.1-1$ Å^{-1} (at $T = 1050$ K) (Ref. 13) [see stars in Fig. 6(b)] and around $k \sim 0.15-0.2$ Å^{-1} (at $T = 295$ K),[15] but also in a very wide range (over a few decades) at smaller k by a picosecond optical technique (at $T = 300$ K),[50] Brillouin light-scattering (at $T = 300$ K),[13,51] and by ultrasonic measurements.[51]

The positions of the spectral-density peaks are very well defined, and the average frequency can be easily associated with the peak position (see Fig. 5) but only limited information about the peak width can be obtained. This is due to the fact that in the frequency range $\lesssim 1$ THz the frequency spectrum is not dense (because of the finite size of the model) and the number of decay channels can be underestimated. The experimental data for the line widths in the IXS experiments shown in Fig. 6(b) by the stars are in very good agreement with our results.

It should be noted that a linear and quadratic dependence of the average frequency and the linewidth, respectively, are quite general features found for structural models of different materials.[18,26,38,44,52–56] A possible explanation of the quadratic dependence of the linewidth on the wave-vector magnitude is given in Ref. 57 in terms of anharmonic effects.

V. TIME EVOLUTION OF PLANE-WAVE EXCITATIONS

Investigation of the spectral densities, as shown in Sec. IV, provides us with indirect estimates of the average frequency and decay time of the propagating plane-wave excitations. The other straightforward way to obtain the average frequency and decay time of plane-wave excitations is to calculate directly the time dependence of the displacement vector, $\mathbf{u}(t)$.

At least two functions can be used to study the decay of plane-wave excitations. The standard way lies in the calculation and analysis of the correlation function (3.19).[47] The correlation function is proportional to the projection of the displacement vector at time t onto the initial plane wave, $A\hat{\mathbf{n}} \cos(\mathbf{k} \cdot \mathbf{r} + \phi_0)$ [see Eq. (3.1)]. The evolution of the correlation function shows how the value of this projection onto a time-invariant $\mathbf{k}$-plane-wave component decays with time (see Fig. 7, where the decay of the correlation functions from

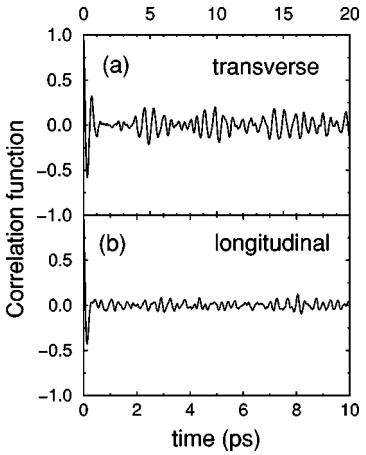

FIG. 7. The correlation function Eq. (3.19) for transverse (a) and longitudinal (b) initial polarizations of plane-wave excitations characterized by the wave-vector magnitude $k \simeq 0.3$ Å^{-1}.

unity at $t=0$ occurs on the time scale $\lesssim 1$ ps). As follows from Eq. (3.19), the time dependence is exactly the back cosine Fourier transform of the spectral-density coefficients. Therefore the analysis performed in Sec. IV is equally applicable to the investigation of the decay of the correlation function and should give the same results for the average frequency and decay time as those obtained directly from time dependencies. Indeed, as seen from Fig. 7, for both polarizations the correlation functions decay and oscillate in qualitative agreement with expression (4.8). The decay times (the typical times at which the envelope of the correlation function drops to zero) estimated from Fig. 7 are $\tau_t \simeq 0.5(0.4)$ ps and $\tau_l \simeq 0.16(0.1)$ ps, agreeing well with the estimates (given in brackets) obtained from fits of the spectral densities by the DHO model.

The other, and from our viewpoint, more appropriate way lies in the investigation of the time evolution of the **k**-plane-wave component, $\mathbf{u}_{\mathbf{kk}}$, defined in Eq. (3.7). The value to be calculated is the projection, $a_{\mathbf{kk}}(t)$ [see Eqs. (3.7) and (3.10)–(3.11)], of the displacement vector, $\mathbf{u}_{\mathbf{k}}(t)$, onto the time-varying **k**-plane-wave component, $A\hat{\mathbf{n}}\cos[\mathbf{k}\cdot\mathbf{r} + \phi_{\mathbf{kk}}(t)]$. The difference between this quantity and the correlation function is related to the appearance of the time-dependent phase in the **k**-plane-wave component. Indeed, if we want to study the decay of the plane-wave excitation characterized by the wave vector **k** at $t=0$ then we should follow the time evolution of the **k**-plane-wave component which not only decays (the amplitude decreases) but also moves (the phase depends on time). Therefore the total displacement vector should be projected onto the moving **k**-plane-wave component.

The evolution of the **k**-plane-wave component is shown in Figs. 8 and 9. We chose the initial plane wave to be a standing wave of cos-type and calculated separately the amplitudes $a_{\mathbf{kk},c}(t)$ and $a_{\mathbf{kk},s}(t)$ of the cos- and sin-like constituents. As clearly seen from Fig. 8(a), $a_{\mathbf{kk},c}(0)=1$ and $a_{\mathbf{kk},s}(0)=0$, but then the sin-like component is activated with time and becomes comparable with the cos-like component. This means that the phase $\phi_{\mathbf{kk}}(t)$ of the **k**-component depends on time [see Figs. 9(a) and 9(b)] and the **k**-plane-wave component is no longer a standing wave but rather a running wave. The running wave moves with the

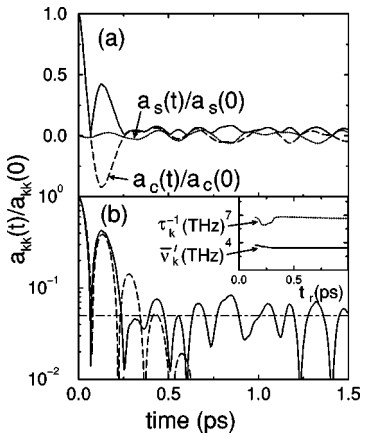

FIG. 8. The amplitude $a_{\mathbf{kk}}(t)/a_{\mathbf{kk}}(0)$ (solid lines) on a linear (a) and semilogarithmic (b) scale versus time for a longitudinal initial plane wave with $k \simeq 0.29$ Å^{-1}. The amplitudes of cos-like (the dashed curve) and sin-like (the dotted curve) constituents are shown in (a). The fit of the time dependence of the amplitude by Eq. (5.4) is shown by the dashed line in (b) while the averaged amplitude $[\overline{a_{\mathbf{kk}}^2(t)}]^{1/2}$ is indicated by the dot-dashed line. The dependence of the fitting parameters $\bar{\nu}_{\mathbf{k}}'$ (the solid line) and $\tau_{\mathbf{k}}$ (the dotted line) in Eq. (5.4) on the upper time limit t_r is shown in the inset in (b).

phase velocity, $v_\phi(t)=[d\phi(t)/dt]/k$, which is a function of time. The phase rate, $d\phi(t)/dt \equiv k v_\phi(t)$, strongly fluctuates in magnitude and changes sign in an apparently chaotic manner [see Figs. 9(a) and 9(b)], so that the **k**-plane-wave component moves in a diffusivelike manner.

The average values of the different powers of phase-rate magnitude, defined as

$$\nu_{\mathbf{k}}^{(n)} \equiv \frac{1}{2\pi}\left[\overline{\left|\frac{d\phi_{\mathbf{kk}}}{dt}\right|^n}\right]^{1/n} = \frac{1}{2\pi}\left[\frac{1}{t}\int_0^t \left|\frac{d\phi_{\mathbf{kk}}}{dt}\right|^n dt\right]^{1/n}, \tag{5.1}$$

where the phase rate is to be found from Eqs. (3.11)–(3.14) (it is proportional to the back sine Fourier transformation of the first moment of the spectral-density coefficients, proportional to $\Sigma_j \omega_j \overline{\alpha_{\mathbf{k}}^j \alpha_{\mathbf{k}',\mathrm{c(s)}}^j} \sin \omega_j t$, and to the back cosine Fourier transformation of the spectral-density coefficients) can

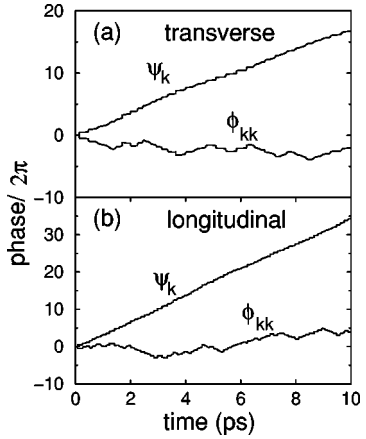

FIG. 9. The phases $\phi_{\mathbf{kk}}(t)$ [see Eq. (3.11)] and $\psi_{\mathbf{k}}(t)$ [see Eq. (5.2)] for longitudinal (a) and transverse (b) initial polarizations of plane waves with $k \simeq 0.29$ Å^{-1}.

be easily numerically averaged over time. Despite the big fluctuations in magnitude of $\phi_{\mathbf{kk}}(t)$, the averaged characteristics (5.1) are well defined. As an example, we have calculated the integral $\psi_{\mathbf{k}}(t)$ of the magnitude of the phase rate [$n=1$ in Eq. (5.1)],

$$\psi_{\mathbf{k}}(t)=\int_0^t \left|\frac{d\phi_{\mathbf{kk}}}{dt}\right| dt, \tag{5.2}$$

and plotted it versus time in Figs. 9(a) and 9(b). The average magnitude of the phase rate, $k\overline{v}_{\phi,\mathbf{k}}$, has then been calculated as the average slope of this curve, which is very close to a straight line.

The averaged magnitude of the phase rate can be related to the average frequency $\overline{\nu}_{\mathbf{k}}$ of the $\mathbf{k}$-plane-wave component according to the following equation:

$$\overline{\nu}_{\mathbf{k}}=\psi_{\mathbf{k}}(t)/t. \tag{5.3}$$

Indeed, the running plane-wave component moves in space backward ($d\phi/dt<0$) and forward ($d\phi/dt>0$) with time, so that $\phi(t)$ is not a monotonic function of time [see Figs. 9(a) and 9(b)] and both the average phase and phase rate are equal to zero. If we consider a similar wave but always moving in one direction (replacing $d\phi/dt$ by $|d\phi/dt|$), then the phase $\psi_{\mathbf{k}}(t)$ is now a monotonic function [see Figs. 9(a) and 9(b)] and the average phase rate $\psi_{\mathbf{k}}(t)/t$, or the average frequency by definition, is not zero. Bearing in mind the equivalence of these two waves from the viewpoint of the definition of the frequency of the running wave, we arrive at Eq. (5.3). The results for $\overline{\nu}_{\mathbf{k}}$ versus different k for transverse and longitudinal polarizations are presented in Figs. 5(a) and 5(b) (the open circles), respectively.

It should be stressed that even for large values of k, where the spectral density is not peak shaped, the value of the averaged magnitude of the phase rate (frequency), $k\overline{v}_{\phi,\mathbf{k}}=\overline{\nu}_{\mathbf{k}}$, is well defined. The dispersion laws, thus obtained, support the estimations made from the fits of the spectral densities by Lorentzians and the DHO model (see Fig. 5). The values of the averaged frequency of the $\mathbf{k}$-plane-wave component calculated from Eqs. (5.2)–(5.3) are not based on any fit and are defined even for the featureless spectral densities at $k\gtrsim 1$ Å^{-1} [see Figs. 2(c) and 2(f)]. This is the advantage of this method as compared to those based on the fitting procedures described in Sec. IV. Note that calculation of the first frequency moments for the spectral densities results in different estimates (by up to 40%) of the average frequencies as compared to those found using Eq. (5.1).

We have shown how the average frequency of the propagating plane-wave excitation can be calculated from the time dependences of the phase. The decay time $\tau_{\mathbf{k}}$ of the propagating plane-wave excitation can also be calculated, but now from the time dependence of the amplitude, $a_{\mathbf{kk}}(t)$ (see Fig. 8). As seen from Fig. 8(a), the amplitude first decays with time and then fluctuates around the average value, $\overline{a^2_{\mathbf{kk}}}$ [see the dot-dashed line in Fig. 8(b)]. The decay time is calculated from the fit of the dependence $a_{\mathbf{kk}}(t)/a_{\mathbf{kk}}(0)$ in the initial stage of relaxation ($t\lesssim t_r$), when the amplitude still does not reach the average value, by the following empirical function [see the dashed line in Fig. 8(b)]:

$$a_{\mathbf{kk}}(t)/a_{\mathbf{kk}}(0)=\exp(-t/\tau_{\mathbf{k}})\left|\cos(2\pi\overline{\nu}'_{\mathbf{k}}t)\right|, \tag{5.4}$$

with $\overline{\nu}'_{\mathbf{k}}$, the frequency in the initial stage of relaxation for $t\lesssim t_r$, and the decay time $\tau_{\mathbf{k}}$ being the fitting parameters. The values of these parameters slightly depend on the upper limit t_r for fitting, as shown in the inset in Fig. 8(b). The data for $\overline{\nu}'_{\mathbf{k}}$ and $\tau_{\mathbf{k}}$ averaged over t_r, the initial phase ϕ_0 in Eq. (3.1), the direction of the polarization vector $\hat{\mathbf{n}}$ in Eq. (3.1) in the case of the transverse polarization, and the direction of the wave vector are shown, respectively, in Fig. 5 (the open squares) and Fig. 6 (the open squares). As follows from these figures, the temporal-decay method gives values of average frequencies quite close to those obtained from the fitting of spectral densities. The same is true for the decay time except in the regions of intermediate and large $k\gtrsim 0.5$ Å^{-1}, where the decay time found by the temporal-decay method is greater, especially than those values obtained by fitting of the spectral densities with the DHO model (see Figs. 6).

VI. ANALYSIS OF THE FINAL STATE FOR THE SCATTERED PLANE WAVE

The decay of the plane-wave excitation can also be characterized via the properties of the final state after decay, averaged over time as $t\to\infty$. An initial plane-wave excitation characterized by the wave vector $\mathbf{k}$ and polarization $\hat{\mathbf{n}}$ is scattered to different plane-wave components characterized by the wave vectors $\mathbf{k}'$ and polarizations $\hat{\mathbf{n}}'$. The distribution $\rho(\mathbf{k}',\hat{\mathbf{n}}'|\mathbf{k},\hat{\mathbf{n}})$ of the weights of different plane-wave components averaged over time in the final state,

$$\rho(\mathbf{k}',\hat{\mathbf{n}}'|\mathbf{k},\hat{\mathbf{n}})\equiv\overline{a^2_{\mathbf{kk}',\hat{\mathbf{n}}\hat{\mathbf{n}}'}(t)}, \tag{6.1}$$

is of particular interest [see Eq. (3.18) where the function from the right-hand side of Eq. (6.1) is evaluated]. Bearing in mind that in Eq. (3.18), $\langle \mathbf{w}^2_{\mathbf{k}',s}\rangle \simeq \langle \mathbf{w}^2_{\mathbf{k}',c}\rangle \simeq \langle \mathbf{w}^2_{\mathbf{k}'}\rangle$ (for finite systems) and that the sum $|\underline{\alpha}^j_{\mathbf{k}',s}|^2+|\underline{\alpha}^j_{\mathbf{k}',c}|^2$ is independent of the phase of cos- and sin-like components defined by Eq. (3.9), expressions (3.18) and (6.1) can be transformed to

$$\rho(\mathbf{k}',\hat{\mathbf{n}}'|\mathbf{k},\hat{\mathbf{n}})\simeq\frac{\sum_j |\overline{\alpha}^j_{\mathbf{k}}|^2|\underline{\alpha}^j_{\mathbf{k}'}|^2}{(\langle \mathbf{w}^2_{\mathbf{k}'}\rangle)^2}. \tag{6.2}$$

The probability for an initial plane wave to be scattered into a plane wave characterized by wave vector $\mathbf{k}'$ and either transverse or longitudinal polarization is given by the total distribution function $\rho_{\mathrm{tot}}(\mathbf{k}'|\mathbf{k},\hat{\mathbf{n}})$,

$$\rho_{\mathrm{tot}}(\mathbf{k}'|\mathbf{k},\hat{\mathbf{n}})=2\rho(\mathbf{k}',\hat{\mathbf{n}}'_{\mathrm{t}}|\mathbf{k},\hat{\mathbf{n}})+\rho(\mathbf{k}',\hat{\mathbf{n}}'_{\mathrm{l}}|\mathbf{k},\hat{\mathbf{n}}), \tag{6.3}$$

where the unit vector $\hat{\mathbf{n}}'_{\mathrm{t}}$ stands for transverse polarization in the final state while $\hat{\mathbf{n}}'_{\mathrm{l}}$ refers to longitudinal polarization, and the factor 2 takes into account the existence of two independent and, in glasses, equivalent transverse polarizations. Glasses are isotropic, and an averaging of Eq. (6.3) over the directions of both initial and final wave vectors (including averaging over transverse polarizations in the initial wave) can be made, resulting in

$$\rho_{\mathrm{tot,t(l)}}(k'|k)=\langle\rho_{\mathrm{tot}}(\mathbf{k}'|\mathbf{k},\hat{\mathbf{n}}_{\mathrm{t(l)}})\rangle_{\Omega_{\mathbf{k},\mathbf{k}'}}. \tag{6.4}$$

In practice, for better statistics, when calculating the distribution functions $\rho_{\mathrm{tot}}(\mathbf{k}'|\mathbf{k},\hat{\mathbf{n}})$, we have also performed an averaging over phases [e.g., ϕ_0 in Eq. (3.1)] and over directions of the polarization vector (for transverse polarization) both in the initial and final states.

If we are interested in the contribution of the same plane-wave $\mathbf{k}$ component as in the initial excitation, then the wave vector $\mathbf{k}'$ should be replaced by $\mathbf{k}$ in Eq. (6.3) and averaging only over $\mathbf{k}$ directions should be made in Eq. (6.4).

First, we consider the final state of a single $\mathbf{k}$-plane-wave component characterized by the same wave vector as the initial one. The phase of this wave has a random value and is not an informative characteristic. The important quantity is the amplitude of the wave, or more precisely its squared average value [see the dot-dashed line in Fig. 8(b)], defined by Eqs. (3.18) and (6.2) at $\mathbf{k}'=\mathbf{k}$,

$$\overline{a^2_{\mathbf{kk}}}\simeq\frac{1}{2}\left\{\frac{\sum_j|\overline{\alpha^j_{\mathbf{k}}}|^2|\underline{\alpha}^j_{\mathbf{k},\mathrm{s}}|^2}{(\langle\mathbf{w}^2_{\mathbf{k},s}\rangle)^2}+\frac{\sum_j|\overline{\alpha^j_{\mathbf{k}}}|^2|\underline{\alpha}^j_{\mathbf{k},\mathrm{c}}|^2}{(\langle\mathbf{w}^2_{\mathbf{k},c}\rangle)^2}\right\}$$

$$\simeq\frac{\sum_j|\overline{\alpha^j_{\mathbf{k}}}|^2|\underline{\alpha}^j_{\mathbf{k}}|^2}{(\langle\mathbf{w}^2_{\mathbf{k}}\rangle)^2}. \tag{6.5}$$

This value can be easily estimated for a peak-shaped spectral density of width Γ. Indeed, the number of eigenmodes contributing to an initial plane wave is $3N\cdot(\Gamma/D)$, where D is the width of the whole vibrational spectrum ($\simeq$40 THz in the case of vitreous silica). Then we can easily evaluate from the normalization conditions Eqs. (3.5) and (3.20) the average value of the spectral-density coefficients in the peak region, $|\overline{\alpha^j_{\mathbf{kk}}}|^2\sim|\underline{\alpha}^j_{\mathbf{kk},\mathrm{s}}|^2\sim(D/\Gamma)\cdot(1/3N)$, and obtain the following estimate for $\overline{a^2_{\mathbf{kk}}}$,

$$\overline{a^2_{\mathbf{kk}}}\sim\frac{D}{\Gamma}\cdot\frac{1}{3N}, \tag{6.6}$$

where we have taken into account that $\langle\mathbf{w}^2_{\mathbf{k}}\rangle\sim1$ according to Eq. (3.5). The factor D/Γ in relation (6.6) shows that the averaged squared amplitude is inversely proportional to the number of initially excited modes and not to all the modes. This factor, being much larger than unity in the long-wavelength regime, decreases with increasing wave-vector magnitude because of the increase of Γ (see Fig. 2) and becomes comparable to unity at $k\gtrsim k_*\simeq1$ Å^{-1} when the peak width is comparable to the full spectral width $\Gamma\sim D$.

Let us consider an initial plane wave characterized by the wave vector $\mathbf{k}$ and polarization $\hat{\mathbf{n}}$. This wave is scattered with time into different plane waves characterized by wave vectors $\mathbf{k}'$ and polarizations $\hat{\mathbf{n}}'$, which do not necessarily coincide with the initial polarization. We would like to know the weights of all plane-wave components in the final state as a function of wave-vector magnitude k'. The distributions of the transverse and longitudinal plane waves, $\rho(\mathbf{k}',\hat{\mathbf{n}}'_{\mathrm{t}}|\mathbf{k},\hat{\mathbf{n}})$ and $\rho(\mathbf{k}',\hat{\mathbf{n}}'_{\mathrm{l}}|\mathbf{k},\hat{\mathbf{n}})$ [see Eq. (6.2)], respectively, and the total distribution, $\rho_{\mathrm{tot}}(\mathbf{k}'|\mathbf{k},\hat{\mathbf{n}})$ [see Eq. (6.3)], for both transverse

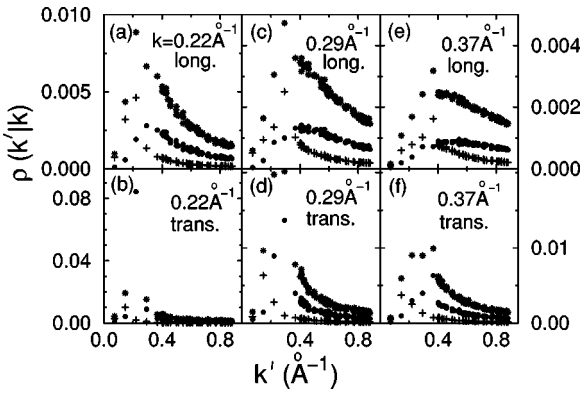

FIG. 10. The distribution functions $\rho(\mathbf{k}',\hat{\mathbf{n}}'_{\mathrm{t}}|\mathbf{k},\hat{\mathbf{n}})$ (circles), $\rho(\mathbf{k}',\hat{\mathbf{n}}'_{\mathrm{l}}|\mathbf{k},\hat{\mathbf{n}})$ (pluses) and $\rho_{\mathrm{av}}(\mathbf{k}'|\mathbf{k},\hat{\mathbf{n}})$ (stars) for longitudinal [(a), (c), and (e)] and transverse [(b), (d), and (f)] initial polarizations of plane waves characterized by different initial wave-vector magnitudes k for the bar-shaped structural model of v-SiO_2. The ordinate scales for (a) and (b) are on the left, and on the right for the other figures.

$\hat{\mathbf{n}}_{\mathrm{t}}$ and longitudinal $\hat{\mathbf{n}}_{\mathrm{l}}$ polarizations of the initial plane-wave excitation are of particular interest. These distributions depend only on the spectral-density coefficients $|\overline{\alpha^j_{\mathbf{k}}}|^2$, $|\underline{\alpha}^j_{\mathbf{k}'}|^2$ and the vibrational spectrum itself and can be easily calculated numerically for different k. The results of such calculations are presented in Fig. 10. The upper (lower) row describes the scattering of initial longitudinal (transverse) plane waves, characterized by different wave-vector magnitudes, into transverse and longitudinal plane waves and also the total distribution of the weights in the final state.

First, we consider scattering of a longitudinal initial wave (the upper row in Fig. 10). The weight distributions $\rho(\mathbf{k}',\hat{\mathbf{n}}'_{\mathrm{l}}|\mathbf{k},\hat{\mathbf{n}}_{\mathrm{l}})$ and $\rho(\mathbf{k}',\hat{\mathbf{n}}'_{\mathrm{t}}|\mathbf{k},\hat{\mathbf{n}}_{\mathrm{l}})$ characterize the scattering of the longitudinal wave to a longitudinal wave, the $\{l\rightarrow l\}$ channel, and of the longitudinal wave to a transverse wave, the $\{l\rightarrow t\}$ channel, respectively. As follows from Fig. 10, these distributions are peak shaped but the positions of the peaks are different. The distribution for the $\{l\rightarrow l\}$ channel has a maximum around $k'_{\mathrm{ll}}\simeq k_{\mathrm{l}}\equiv k$ (or maybe a bit below the initial wave vector), while the distribution for the $\{l\rightarrow t\}$ channel is mainly concentrated at a higher wave-vector value, $k'_{\mathrm{lt}}>k_{\mathrm{l}}$. The total distribution, $\rho_{\mathrm{tot}}(\mathbf{k}'|\mathbf{k},\hat{\mathbf{n}}_{\mathrm{l}})$, in the final state is a sum of double the distribution for the $\{l\rightarrow t\}$ channel and the distribution for the $\{l\rightarrow l\}$ channel. If the peaks related to the individual channels and constituting the total distribution are narrow enough, then the distribution function $\rho_{\mathrm{tot}}(\mathbf{k}'|\mathbf{k},\hat{\mathbf{n}}_{\mathrm{l}})$ is double-peaked (not clearly seen in Fig. 10). If the peaks are too wide, then $\rho_{\mathrm{tot}}(\mathbf{k}'|\mathbf{k},\hat{\mathbf{n}}_{\mathrm{l}})$ looks like a single wide peak (see Fig. 10) with a maximum position $k'_{\mathrm{l,tot}}$ close to k'_{lt}.

Such a shape of the distributions of the weights of plane waves in the final state can be qualitatively understood in the following way. The distribution function $\rho(\mathbf{k}',\hat{\mathbf{n}}'_{\mathrm{t}}|\mathbf{k},\hat{\mathbf{n}}_{\mathrm{l}})$ of the transverse waves is an integral (sum in the case of a finite-size model) of the product of two spectral-density coefficients, $|\overline{\alpha^j_{\mathbf{k},\hat{\mathbf{n}}_{\mathrm{l}}}}|^2$ for longitudinal and $|\underline{\alpha}^j_{\mathbf{k}',\hat{\mathbf{n}}'_{\mathrm{t}}}|^2$ for transverse polarization. In the acoustic regime, these peak-shaped

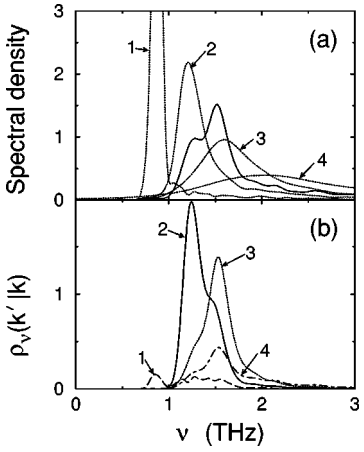

FIG. 11. (a): The spectral densities $\overline{S_{\mathbf{k}}}(\nu)$ for a longitudinal initial plane wave with $k \simeq 0.15$ Å^{-1} (solid line) and $\overline{S'_{\mathbf{k}}}(\nu)$ for the transverse final plane-wave components characterized by different $k' \simeq 0.15$ Å^{-1} (curve 1), 0.22 Å^{-1} (curve 2), 0.29 Å^{-1} (curve 3), 0.37 Å^{-1} (curve 4). (b) The functions $\rho_\nu(\mathbf{k}', \hat{\mathbf{n}}'_t | \mathbf{k}, \hat{\mathbf{n}}_l)$ which are related to the products of the spectral-density coefficients according to the relation $\rho_\nu(\mathbf{k}', \hat{\mathbf{n}}'_t | \mathbf{k}, \hat{\mathbf{n}}_l) = (1/3N)\Sigma_j \rho_j(\mathbf{k}', \hat{\mathbf{n}}'_t | \mathbf{k}, \hat{\mathbf{n}}_l)\, \delta(\nu - \nu^j) = (1/3N)\Sigma_j |\overline{\alpha^j_{\mathbf{k}, \hat{\mathbf{n}}_l}}|^2 \cdot |\underline{\alpha}^j_{\mathbf{k}', \hat{\mathbf{n}}'_t}|^2 \delta(\nu - \nu^j)$. The initial-state spectral-density coefficient $|\overline{\alpha^j_{\mathbf{k}, \hat{\mathbf{n}}_l}}|^2$, corresponds to the solid line in (a) while the final-state spectral-density coefficients $|\underline{\alpha}^j_{\mathbf{k}', \hat{\mathbf{n}}'_t}|^2$ correspond to the dotted curves in (a) [denoted by the same numbers in (a) as their products in (b)].

spectral densities have maxima at $\nu_l \simeq c_l k/2\pi$ and $\nu'_t \simeq c_t k'/2\pi$, respectively, which generally do not coincide with each other. In Fig. 11(a), as an example we show the spectral density for an initial longitudinal wave at $k \simeq 0.15$ Å^{-1} (solid line) and a few spectral densities for transverse waves in the final state (dotted lines) characterized by $k' \simeq 0.15$ Å^{-1} (curve 1), 0.22 Å^{-1} (curve 2), 0.29 Å^{-1} (curve 3), and 0.37 Å^{-1} (curve 4). The distribution function $\rho(\mathbf{k}', \hat{\mathbf{n}}'_t | \mathbf{k}, \hat{\mathbf{n}}_l)$ has a maximum at the value $\mathbf{k}'$, such that the product of the spectral-density coefficients $\rho_j(\mathbf{k}', \hat{\mathbf{n}}'_t | \mathbf{k}, \hat{\mathbf{n}}_l) = |\overline{\alpha^j_{\mathbf{k}, \hat{\mathbf{n}}_l}}|^2 \cdot |\underline{\alpha}^j_{\mathbf{k}', \hat{\mathbf{n}}'_t}|^2$ is maximal in the peak regions of the spectral densities. The latter condition is obeyed if the peaks of the two spectral densities lie approximately in the same frequency region, i.e., $\nu_l \simeq \nu'_t$ [see, e.g., curves 2 and 3 covering the same region as the solid line in Fig. 11(a)]. When we plot $\rho_j(\mathbf{k}', \hat{\mathbf{n}}'_t | \mathbf{k}, \hat{\mathbf{n}}_l)$ versus frequency [Fig. 11(b)], indeed we see that the maximum area lies under curves (2) and (3) obtained by multiplication of the corresponding curves by the solid line in Fig. 11(a). Therefore the distribution $\rho(\mathbf{k}', \hat{\mathbf{n}}'_t | \mathbf{k}, \hat{\mathbf{n}}_l)$ has a maximum around k'_{lt} satisfying the equation $\nu_l \simeq c_l k/2\pi \simeq c_t k'_{lt}/2\pi \simeq \nu'_t$, i.e.,

$$k'_{lt} \simeq c_l k/c_t, \tag{6.7}$$

which is obviously greater than the wave vector of the initial longitudinal wave.

The distribution of longitudinal waves for the $\{l \to l\}$ channel can be analyzed in a similar manner. The main difference from the $\{l \to t\}$ channel is that the spectral density of the longitudinal plane wave in the final state coincides with the spectral density of the initial longitudinal plane wave at approximately the same wavevector magnitude as for the initial wave,

$$k'_{ll} \simeq k. \tag{6.8}$$

Actually, the value k'_{ll} should be slightly shifted to lower values, because the height of the peak for the spectral-density coefficients $|\underline{\alpha}^j_{\mathbf{k}'}|^2$ increases with decreasing k' and the maximum of the product of the spectral densities is reached in the low-frequency tail of the spectral density for the initial plane wave.

The scattering of an initially transverse plane wave occurs similarly. In particular, the conclusion that the average frequency, ν', of the majority of the plane-wave components comprising the final state coincides with the average frequency ν of the initial plane wave,

$$\nu' \simeq \nu, \tag{6.9}$$

holds true independently of the polarization of the initial plane-wave excitation. Therefore we can roughly say that the disorder-induced scattering of the plane wave is approximately ''elastic'' (on average). This is not an absolutely precise conclusion because, first, the plane-wave components are distributed in frequency (composed of eigenmodes having different frequencies) in the initial and final states and, second, even the maximum of the distribution in the final state is slightly shifted to lower frequencies as compared to the initial one, as discussed above.

In the case of the scattering of the initial transverse plane wave, two channels are available: $\{t \to l\}$ and $\{t \to t\}$. The distribution functions $\rho(\mathbf{k}', \hat{\mathbf{n}}'_l | \mathbf{k}, \hat{\mathbf{n}}_t)$ and $\rho(\mathbf{k}', \hat{\mathbf{n}}'_t | \mathbf{k}, \hat{\mathbf{n}}_t)$ of the weights of plane waves in the final state for these channels have peaks located around the following values:

$$k'_{tl} \simeq c_t k/c_l \quad \text{and} \quad k'_{tt} \simeq k. \tag{6.10}$$

As follows from Eq. (6.10) and Figs. 10(b), 10(d), and 10(f), the peak for longitudinal waves lies below the initial k, while for transverse waves the peak approximately coincides with k, being slightly shifted to smaller values for reasons similar to those discussed above for the $\{l \to l\}$ channel.

VII. LOW-DIMENSIONAL MODEL

One way to overcome the disadvantages of finite-size three-dimensional (3D) numerical models is to analyze low-dimensional models. Much lower wave vectors $k \gtrsim k^{(d)}_{\min} = 2\pi/N^{1/d}a$ (with a being a typical interatomic distance and N the number of atoms) are available, for example, in one-dimensional ($D=1$) models as compared to the 3D case, and the acoustic spectrum appears to be much more dense. In order to check and support the analytical and numerical approaches presented above for the 3D case, we have performed numerical experiments for a disordered 1D model and calculated the distribution function $\rho(\mathbf{k}', \hat{\mathbf{n}}' | \mathbf{k}, \hat{\mathbf{n}})$ for it.

A ''zigzag'' linear chain (along the x direction) of atoms [see the inset in Fig. 12(b)], positionally ordered in the x-y plane, has been chosen as a model. The atoms of two types ($i=1,2$), characterized by the masses m_i are in equilibrium positioned at $\{x_i/a, y_i/a\}$ (e.g., we used the coordinates $\{0,0\}$ and $\{0.4,0.5\}$ for the first and second atom, respec-

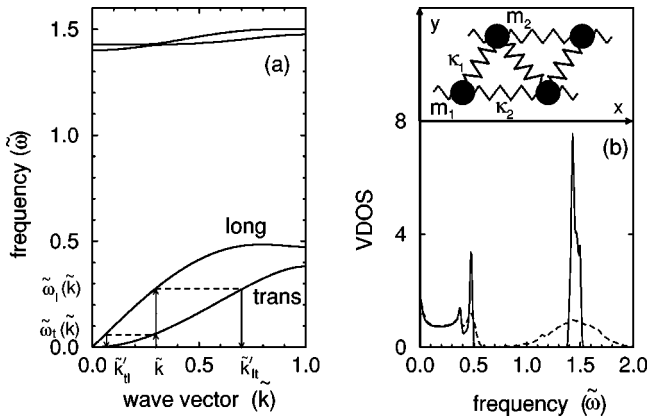

FIG. 12. (a): Dispersion curves [$\tilde{\omega}=\omega\sqrt{m/\kappa_1}$ vs $\tilde{k}=k/(\pi/a)$] for a 1D zigzag chain model [see the inset in (b)] characterized by the following parameters: the equilibrium coordinate of atoms in the unit cell, $x_1/a=0$; $y_1/a=0$, $x_2/a=0.4$; $y_2/a=0.5$, ratio of force constants $\kappa_2/\kappa_1=0.1$, masses $m_1=m_2=m$, and the total number of atoms $N=2000$. The arrows mark the initial wave-vector magnitude $\tilde{k}$ and final wave-vector values $\tilde{k}'_{tl}$ and $\tilde{k}'_{lt}$ (see text). (b): The VDOS of the linear zigzag chain model with the same set of parameters as in (a) (solid line) together with that for a disordered chain with fluctuations in force constants $\delta\kappa_1/\kappa_1=0.3$, $\delta\kappa_2/\kappa_2=0.3$ (dashed line).

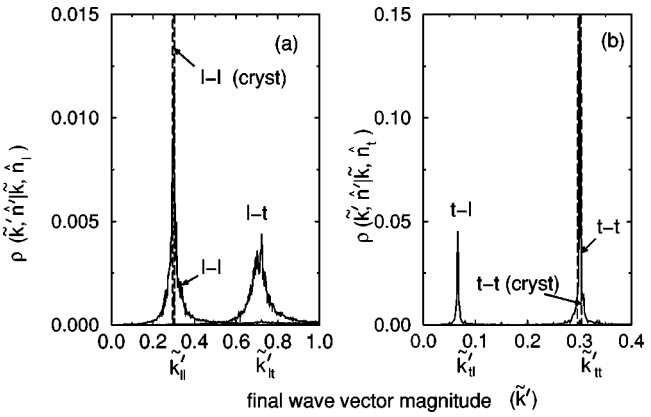

FIG. 13. The distribution functions $\rho(\tilde{\mathbf{k}}',\hat{\mathbf{n}}'|\tilde{\mathbf{k}},\hat{\mathbf{n}})$ for different scattering channels (as marked in the figure), for (a) longitudinal ($\hat{\mathbf{n}}=\hat{\mathbf{n}}_l$) and (b) transverse ($\hat{\mathbf{n}}=\hat{\mathbf{n}}_t$) initial polarizations of plane waves characterized by initial wave-vector magnitudes $\tilde{k}=k/(\pi/a)=0.3$ for an ordered (dashed lines) and disordered (solid lines) linear zigzag chain model characterized by the same parameters as in Fig. 12. The dashed lines corresponding to the $\{l\rightarrow t\}$ scattering channel in (a) and $\{t\rightarrow l\}$ scattering channel in (b) for the crystalline (ordered) chain cannot be seen because they coincide with the abscissa, since for them $\rho(\tilde{\mathbf{k}}',\hat{\mathbf{n}}'|\tilde{\mathbf{k}},\hat{\mathbf{n}})$ is effectively zero.

tively; the second atom is displaced from the middle of the unit cell, $x_2\neq 0.5$, in order to avoid the extended Brillouin zone for $m_1=m_2$) in the unit cell of size a, which is periodically repeated $N/2$ times with periodic boundary conditions. The nearest neighbors of different types are connected by springs of force constant κ_1 while the nearest neighbors of the same type are connected by springs with force constant κ_2. Such a model is one of the simplest in 1D to show both the longitudinal and transverse acoustic branches that we need for our consideration. The dispersion curves and VDOS for the crystalline chain are presented in Figs. 12(a) and 12(b). The $\omega^{-1/2}$-singularity in the VDOS at $\omega\rightarrow 0$ [see Fig. 12(b)] is due to the parabolic dispersion law for the transverse acoustic phonons in the long-wavelength limit, $\omega_t\propto k^2$ [see Fig. 12(a)], which is typical for transverse vibrations of a linear chain. Disorder then has been introduced in the system by randomly distributing spring constants around their mean values $\overline{\kappa_1}$ and $\overline{\kappa_2}$ according to a normal distribution with variances $\delta\kappa_1$ and $\delta\kappa_2$, respectively. The VDOS of the disordered chain is shown by the dashed curve in Fig. 12(b). For the parameters of the model used, the VDOS in the acoustic regime is not changed appreciably by disorder.

Our main purpose here in analysing the vibrations of a disordered 1D chain is to calculate the distribution function $\rho(\mathbf{k}',\hat{\mathbf{n}}'|\mathbf{k},\hat{\mathbf{n}})$ characterizing the scattering of a plane-wave excitation. First, we have calculated this distribution function for the crystalline counterpart ($\delta\kappa_i=0$) and not surprisingly (a detailed analysis will be given elsewhere) we found for $k\leqslant\pi/a$ only $\{t\rightarrow t\}$ and $\{l\rightarrow l\}$ channels [see the dashed lines in Figs. 13(a) and 13(b) marking the peaks at $k'_{tt}=k$ and $k'_{ll}=k$ for the $\{t\rightarrow t\}$ and $\{l\rightarrow l\}$ channels, respectively]. Disorder changes the situation dramatically and gives rise to the occurrence of $\{t\rightarrow l\}$ and $\{l\rightarrow t\}$ channels [see the solid lines in Figs. 13(a) and 13(b)] in complete agreement with the results of the k analysis given in Fig. 10. The positions of the additional peaks, at k'_{tl} ($\{t\rightarrow l\}$ channel) and k'_{lt} ($\{l\rightarrow t\}$ channel), can be obtained from the crystalline dispersion laws for the 1D chain by solving the equations: $\omega_t(k)=\omega_l(k'_{tl})$ and $\omega_l(k)=\omega_t(k'_{lt})$, respectively [see arrows in Fig. 12(a)]. The width of the peaks increases with increasing disorder. We have also found a similar shape of the distribution function ρ (for four channels) for all wave vectors $k\leqslant\pi/a$ with corresponding ω_t and ω_l lying in the range of the dense spectrum. Therefore the results of this computer experiment on the 1D model fully support the k analysis presented in Sec. VI.

VIII. SCATTERING MECHANISM

From numerical calculations for both the 1D linear chain model and the 3D model of v-SiO_2, we have found that plane waves scatter not only to modes of approximately the same wavelength but also to modes of rather different wavelength but of similar frequency. The reason for such scattering is a natural question.

First, we consider the 1D linear chain model. As can be seen from Fig. 12(b), the VDOS of the disordered chain in the acoustic regime (for the chosen set of parameters) is hardly different from the VDOS of the crystalline counterpart. This means that, in this case, force-constant disorder does not create or remove many vibrational states from the acoustic frequency range. Hence the appearance of the $\{t\rightarrow l\}$ and $\{l\rightarrow t\}$ channels should be explained in terms of existing transverse and longitudinal acoustic waves. Indeed, in a crystal, long-wavelength plane waves decay into phonons with the same wave vector because of quasimomentum conservation. Therefore a wave with the same frequency but different type of polarization cannot be excited. Disorder destroys the quasimomentum conservation (the wave vector is no longer a good quantum value) and new channels for scattering are opened. A plane-wave excitation decays into eigenmodes having approximately the same frequency as

that of the plane wave having nonzero overlap integrals with this plane wave. Due to disorder, such overlaps are finite for all the eigenstates within a typical interaction scale independent of their polarization (transverse or longitudinal) and dominant wave vector. Therefore an original plane wave, independent of its polarization, is scattered into both transverse and longitudinal plane waves. This gives a qualitative explanation of the existence of $\{t \rightarrow l\}$ and $\{l \rightarrow t\}$ scattering channels.

In the 3D case, the situation can be more complicated. Apart from the scattering mechanism due to the disorder-induced mixing of transverse and longitudinal plane waves discussed above, extra states (comprising the Boson peak) relative to the Debye spectrum (e.g., optic modes pushed down by disorder[58,59]) could participate in the hybridization between plane waves with different polarizations.

IX. CONCLUSIONS

We have demonstrated how the evolution of an initially plane-wave vibrational excitation in an amorphous solid can be investigated in time, frequency, and momentum spaces. Analysis in **k** space is particularly informative, and evidence for scattering between longitudinal and transverse channels, and vice versa, has been obtained from numerical simulations for vitreous silica, as well as a ''toy'' model (zigzag chain in the plane with force-constant disorder).

In discussing the limitations of the present approach, we would like to note that only disorder-induced decay channels of the plane-wave excitations have been analyzed here. The results are formally obtained at zero temperature and are temperature independent in the harmonic approximation under consideration. We believe that our approach is adequate in a particular temperature range $T_{\min} \lesssim T \lesssim T_{\max}$ in real glasses. At low temperatures, $T \lesssim T_{\min}$, decay via two-level systems could be important,[4,27,28] while at higher temperatures ($T \gtrsim T_{\max}$) around the glass transition, anharmonic channels could dominate.[25] In the particular case of vitreous silica, the relevant temperature range is $100 \lesssim T \lesssim 1000$ K, where the mean free path is practically temperature independent.[29]

[1] *Scattering and Localization of Classical Waves in Random Media*, edited by P. Sheng (World Scientific, Singapore, 1990).
[2] P. Sheng, *Introduction to Wave Scattering, Localization, and Mesoscopic Phenomena* (Academic Press, San Diego, 1995).
[3] P. Sheng, M. Zhou, and Z.-Q. Zhang, Phys. Rev. Lett. **72**, 234 (1994).
[4] U. Buchenau, Yu. M. Galperin, V. L. Gurevich, D. A. Parshin, M. A. Ramos, and H. R. Schober, Phys. Rev. B **46**, 2798 (1992).
[5] P. B. Allen and J. Kelner, Am. J. Phys. **66**, 497 (1998).
[6] P. Tong, B. Li, and B. Hu, Phys. Rev. B **59**, 8639 (1999).
[7] R. Dell'Anna, G. Ruocco, M. Sampoli, and G. Viliani, Phys. Rev. Lett. **80**, 1236 (1998).
[8] F. Sette, G. Ruocco, M. Krisch, U. Bergmann, C. Masciovecchio, V. Mazzacurati, G. Signorelli, and R. Verbeni, Phys. Rev. Lett. **75**, 850 (1995).
[9] G. Ruocco, F. Sette, U. Bergmann, M. Krisch, C. Masciovecchio, V. Mazzacurati, G. Signorelli, and R. Verbeni, Nature (London) **379**, 521 (1996).
[10] C. Masciovecchio, G. Ruocco, F. Sette, M. Krisch, R. Verbeni, U. Bergmann, and M. Soltwisch, Phys. Rev. Lett. **76**, 3356 (1996).
[11] U. Buchenau, C. Pecharroman, R. Zorn, and B. Frick, Phys. Rev. Lett. **77**, 659 (1996).
[12] M. Foret, E. Courtens, R. Vacher, and J.-B. Suck, Phys. Rev. Lett. **77**, 3831 (1996).
[13] P. Benassi, M. Krisch, C. Masciovecchio, V. Mazzacurati, G. Monaco, G. Ruocco, F. Sette, and R. Verbeni, Phys. Rev. Lett. **77**, 3835 (1996).
[14] U. Buchenau, A. Wischnewski, D. Richter, and B. Frick, Phys. Rev. Lett. **77**, 4035 (1996).
[15] C. Masciovecchio, G. Ruocco, F. Sette, P. Benassi, A. Cunsolo, M. Krisch, V. Mazzacurati, A. Mermet, G. Monaco, and R. Verbeni, Phys. Rev. B **55**, 8049 (1997).
[16] A. Wischnewski, U. Buchenau, A. J. Dianoux, W. A. Kamitakahara, and J. L. Zarestky, Phys. Rev. B **57**, 2663 (1998).
[17] C. Masciovecchio, G. Monaco, G. Ruocco, F. Sette, A. Consulo, M. Krisch, A. Mermet, M. Soltwisch, and R. Verbeni, Phys. Rev. Lett. **80**, 544 (1998).
[18] M. Alvarez, F. J. Bermejo, P. Verkerk, and B. Roessli, Phys. Rev. Lett. **80**, 2141 (1998).
[19] G. Monaco, C. Masciovecchio, G. Ruocco, and F. Sette, Phys. Rev. Lett. **80**, 2161 (1998).
[20] M. Foret, B. Hehlen, G. Taillades, E. Courtens, R. Vacher, H. Casalta, and B. Dorner, Phys. Rev. Lett. **81**, 2100 (1998).
[21] E. Rat, M. Foret, E. Courtens, R. Vacher, and M. Arai, Phys. Rev. Lett. **83**, 1355 (1999).
[22] A. Fontana, R. Dell'Anna, M. Montagna, F. Rossi, G. Viliani, G. Ruocco, M. Sampoli, U. Buchenau, and A. Wischnewski, Europhys. Lett. **47**, 56 (1999).
[23] P. B. Allen and J. L. Feldman, Phys. Rev. B **48**, 12 581 (1993).
[24] J. L. Feldman, M. D. Kluge, P. B. Allen, and F. Wooten, Phys. Rev. B **48**, 12 589 (1993).
[25] J. Fabian and P. B. Allen, Phys. Rev. Lett. **77**, 3839 (1996).
[26] J. L. Feldman, P. B. Allen, and S. R. Bickham, Phys. Rev. B **59**, 3551 (1999).
[27] P. Sheng and M. Zhou, Science **253**, 539 (1991).
[28] E. Gaganidze, R. Konig, P. Esquinazi, K. Zimmer, and A. Burin, Phys. Rev. Lett. **79**, 5038 (1997).
[29] R. Vacher, J. Pelous, and E. Courtens, Phys. Rev. B **56**, R481 (1997).
[30] J. Horbach, W. Kob, and K. Binder, J. Non-Cryst. Solids **235**, 320 (1998).
[31] J. Horbach, W. Kob, and K. Binder, J. Phys. Chem. B **103**, 4104 (1999).
[32] A. A. Maradudin, E. W. Montroll, G. H. Weiss, and I. P. Ipatova, *Theory of Lattice Dynamics in the Harmonic Approximation* (Academic Press, New York, 1971).
[33] G. Leibfried and N. Breuer, *Point Defects in Metals I. Introduction to the Theory* (Springer, Berlin, 1978).
[34] P. H. Dederichs and R. Zeller, in *Point Defects in Metals II. Dynamical Properties and Diffusion Controlled Reactions* (Springer, Berlin, 1980).
[35] M. I. Klinger, Phys. Rep. **165**, 275 (1988).
[36] Yu. M. Galperin, V. G. Karpov, and V. I. Kozub, Adv. Phys. **38**, 669 (1989).

[37] W. Schirmacher, G. Diezemann, and C. Ganter, Phys. Rev. Lett. **81**, 136 (1998).
[38] J. Hafner and M. Crajci, J. Phys.: Condens. Matter **6**, 4631 (1994).
[39] S. N. Taraskin and S. R. Elliott, following paper, Phys. Rev. B **61**, 12 031 (2000).
[40] B. W. H. van Beest, G. J. Kramer, and R. A. van Santen, Phys. Rev. Lett. **64**, 1955 (1990).
[41] Y. Guissani and B. Guillot, J. Chem. Phys. **104**, 7633 (1995).
[42] K. Vollmayr, W. Kob, and K. Binder, Phys. Rev. B **54**, 15 808 (1996).
[43] S. N. Taraskin and S. R. Elliott, Phys. Rev. B **56**, 8605 (1997).
[44] R. Fernandez-Perea, F. J. Bermejo, and E. Enciso, Phys. Rev. B **53**, 6215 (1996).
[45] S. R. Elliott, *Physics of Amorphous Materials*, 2nd ed. (Longman, New York, 1990).
[46] H. Ehrenreich and L. M. Schwarts, in *Solid State Physics*, edited by H. Ehrenreich, F. Seitz, and D. Turnbull (Academic, New York, 1976), Vol. 31, p. 149.
[47] J.-P. Hansen and I. R. McDonald, *Theory of Simple Liquids*, 2nd ed. (Academic Press, London, 1990).
[48] M. T. Dove, M. J. Harris, A. C. Hannon, J. M. Parker, I. P. Swainson, and M. Gambhir, Phys. Rev. Lett. **78**, 1070 (1997).
[49] F. Terki, C. Levelut, M. Boissier, and J. Pelous, Phys. Rev. B **53**, 2411 (1996).
[50] T. C. Zhu, H. J. Maris, and J. Tauc, Phys. Rev. B **44**, 4281 (1991).
[51] R. Vacher, J. Pelous, F. Plicque, and A. Zarembowitch, J. Non-Cryst. Solids **45**, 397 (1981).
[52] G. S. Grest, S. R. Nagel, and A. Rahman, Phys. Rev. Lett. **49**, 1271 (1982).
[53] H. R. Schober and B. B. Laird, Phys. Rev. B **44**, 6746 (1991).
[54] V. Mazzacurati, G. Ruocco, and M. Sampoli, Europhys. Lett. **34**, 681 (1996).
[55] S. N. Taraskin and S. R. Elliott, Europhys. Lett. **39**, 37 (1997).
[56] M. C. C. Ribeiro, M. Wilson, and P. A. Madden, J. Chem. Phys. **108**, 9027 (1998).
[57] J. Fabian and P. B. Allen, Phys. Rev. Lett. **82**, 1478 (1999).
[58] S. N. Taraskin and S. R. Elliott, J. Phys.: Condens. Matter **11**, A219 (1999).
[59] S. N. Taraskin and S. R. Elliott, Phys. Rev. B **59**, 8572 (1999).